Aging exacerbates the brain inflammatory micro-environment contributing to α-synuclein pathology and functional deficits a mouse model of DLB/PD

Michiyo Iba
National Institute on Aging, National Institutes of Health
Ross McDevitt
National Institute on Aging
Changyoun Kim
National Institute on Aging, National Institutes of Health https://orcid.org/0000-0001-9936-8195
Roshni Roy
National Institute on Aging, National Institutes of Health
Dimitra Sarantopoulou
National Institute on Aging, National Institutes of Health
Ella Tommer
National Institute on Aging, National Institutes of Health
Somin Kwon
National Institute on Aging, National Institutes of Health
Byron Siegars
National Institute on Aging, National Institutes of Health
Michelle Sallin
National Institute on Aging, National Institutes of Health
Jyoti Sen
National Institute on Aging, National Institutes of Health
Ranjan Sen
National Institute on Aging, National Institutes of Health
Eliezer Masliah (eliezer.masliah@nih.gov)
National Institute on Aging, National Institutes of Health

Article

Keywords: -synuclein, aging, Parkinson's disease, Dementia with Lewy bodies, preformed fibrils, inflammation, T cell infiltration, microglia, RNA-seq, neurodegeneration.

Posted Date: February 19th, 2021

DOI: https://doi.org/10.21203/rs.3.rs-211252/v1

Abstract

-synuclein (-syn) progressively accumulates in age related neurodegenerative diseases such as Parkinson's disease (PD) and Dementia with Lewy bodies (DLB). Although -syn spreading has been extensively investigated, the role of aging in the manifestation of disease remains unclear. Thus, we explored the role of aging in the pathogenesis of synucleinopathies in a mouse model of DLB/PD initiated by intrastiatal injection of -syn preformed fibrils (pff). We found that aged mice showed more extensive accumulation of -syn and behavioral deficits that was associated with greater infiltration of T cells and microgliosis. Microglial inflammatory gene expression induced by -syn-pff injection in young mice had hallmarks of aged microglia, indicating that enhanced age-associated pathologies may result from inflammatory synergy between aging and the effects of -syn aggregation. We propose that aging related inflammation influences outcomes of pathological spreading of -syn and suggests that targeting immune responses might be important in developing treatments for DLB/PD.

Introduction

Age is the main risk factor for neurodegenerative disorders with dementia and movement dysfunction including Alzheimer's Disease (AD), Dementia with Lewy bodies (DLB) and Parkinson's Disease (PD) [1]. While in AD, amyloid beta (Aβ), and tau play a central role, in DLB and PD -synuclein (-syn) is a key mediator [2-6]. However, -syn has been shown to accumulate in the brains during aging and in AD and in DLB, Aβ and tau are also found in conjunction with -syn in selected brain regions [7-9].

Aging is associated with deficits in proteostasis, immune surveillance and stem cell regeneration and increased DNA damage and methylation, mitochondrial dysfunction and formation of senescent cells [10-13]. It is hypothesized that while alterations in protein homeostasis during aging might be associated with progressive accumulation of Aβ, tau and -syn [14] the other hallmark pathways of aging such as neuroinflammation and cell senescence might interact with protein aggregation to lead to neurodegeneration [13]. Under physiological conditions -syn is an intracellular protein that might play a role in neuroplasticity [15], however during aging and under pathological conditions -syn aggregates can be released to the extracellular space leading to cell to cell propagation [16,17] spreading and seeding of small aggregates into preformed protofibrils (pff) [18,19] and fibrils in neighboring neuronal and non-neuronal cells [20]. Recent evidences have shown that the intrinsic structure of -syn fibrils dictates the characteristic of the synucleinopathies [21] and for instance inoculation of selected -syn pff's into the CNS can reproduce several aspects of the pathology of DLB/PD in wild type animals models [19,21].

Althought protein aggregation and spreading has been extensively studied less is known about the contribution of aging. One possibility by which ageing might lead to neurodegeneration is dysregulation in immune cell function [22-25]. This might be in part mediated by extracellular -syn propagating to glial cells [26-28]. For example, it has been shown that -syn can activate innate immune responses via Toll like

receptors [26,29-33]. Recent studies have also shown that in DLB/PD [34,35] as well as in animal models [36,37] □-syn might trigger inflammatory responses involving T cells.

In this study we evaluated the role of aging in neurodegeneration in the □-syn pff model. We found that inoculation of pffs in aged mice resulted in greater spreading and deficits compared to young mice with □-syn pff-inducing genes networks in young mice that overlaped with genes differentially expressed in aged mice. We propose that such changes in inflammatory gene expression underlies the increased susceptibility of aged mice to enhanced □-syn induced pathology.

Results

Inoculation of □-syn pff in aged mice resulted in enhanced accumulation and associated deficits compared to young mice

Previous studies have shown that □-syn pff injection induces neuropathological features associated with DLB/PD [18,19]. To investigate the effects of aging on the □-syn neuropathology and related deficits, first we injected □-syn pff into striatum of young mouse cohort and examined □-syn distribution and dissemination at 1- and 3-months after injection. As expected, the control (PBS) injected mice did not show the characteristic □-syn pathology in any brain region when immunostained with the antibody against phosphorylated □-syn (p-□-syn) (Fig. 1A, C, E and G, left panels). In contrast, the □-syn pff injected young mice showed Lewy body like p-□-syn pathology mainly in the neocortex and amygdala and Lewy neurite like p-□-syn positive pathology in the neuropil in the striatum at 1-month after injection (Fig. 1A). At 3-months after injection, we observed more robust p-□-syn pathology in all neocortex, amygdala and striatum (Fig. 1C). Image analysis of p-□-syn percentage area of neuropil showed significant increase of p-□-syn in the □-syn pff injected young mice at 1- and 3-month after injection compare to the PBS injected young mice (Figs. 1B, D).

Next, we injected □-syn pff into striatum of 18–19 months old mice to test if aging affects transmission of □-syn pathology and analyzed the brains at 1- and 3-month after injection. Intracranial injection of □-syn pff into aged mice induced robust p-□-syn pathology in the neocortex, amygdala and striatum at 1-month (Fig. 1E) and 3-month post injection (Fig. 1G). Image analysis of p-□-syn percentage area of neuropil showed significant increase of p-□-syn in the □-syn pff injected aged mice at 1- and 3-month after injection compare to the PBS injected aged mice in all brain regions (Fig. 1F and H). Comparison of p-□-syn percentage area of neuropil between young and aged mouse cohorts revealed that the aged mouse cohort showed higher percentage of p-□-syn neuropil in the neocortex, amygdala and striatum at both 1- and 3-month after injection (Figs. 1I-K).

Then, we characterized the effects of aging on behavioral tests in this model. The distance traveled in the open field test, there were main effects of □-syn ($F_{1,85} = 6.15$, $p = 0.015$), material x sex interaction ($F_{1,85} = 6.95$; $p = 0.010$), and material x interval x age interaction ($F_{1,85} = 9.61$, $p = 0.0026$) (Figs. 2A, B). Post-hoc comparisons in young mice revealed differences between PBS and □-syn pff injected mice at 1-month

post-injection ($p < 0.05$). In the aged mice, there were only differences caused by □-syn pff injections at 3 months ($p < 0.05$) (Fig. 2A). Further analysis within the aged mice showed that the effects were driven exclusively in females, where 3-month □-syn pff mice differed from PBS ($p < 0.01$) (Fig. 2B). In the fear conditioning test, freezing to the cue was significantly affected by □-syn pff ($F(1,85) = 4.61$, $p = 0.035$). This effect was driven primarily through aged mice, where □-syn pff injections significantly reduced freezing vs PBS control at 3 months post-injection ($p < 0.05$) (Fig. 2C). To account for inter-mouse variability in freezing behavior, we examined the ratio of freezing to cue : context. Here the main effect of □-syn pff was more pronounced ($F(1,85) = 7.64$,$p = 0.0070$), and there was a marginally significant □-syn pff x age x sex interaction ($F1,85 = 3.96$, $p = 0.050$). □-syn pff significantly reduced this ratio at 3 months post-injection in aged females ($p < 0.05$) and in all aged mice combined ($p < 0.01$) (Fig. 2D). There were no significant main or interacting effects of material on freezing during training baseline (Figure S2A) or on contextual testing day (Figure S2B).

In the wire hang test, there were significant main effects of material ($F1,85 = 5.72$, $p = 0.019$) and a □-syn pff x sex interaction ($F1,85 = 5.59$, $p = 0.020$). To combine data within sexes across different ages, which were highly different ($F1,85 = 98.58$, $p = 7e\text{-}16$), we normalized each mouse's measurement to percent of age/sex/batch matched controls. Within all combined male mice, there was a progressive decline in performance with significant differences in the □-syn pff group when compared to PBS controls at 1 month ($p < 0.05$) and 3 months ($p < 0.001$) after □-syn pff injection (Figure S1C). Within the combined female population there was no difference between PBS and □-syn pff injected mice (Figure S1D). In rotarod, there was a main effect of □-syn ($F(1,85) = 7.01$, $p = 0.0097$). However, when post-hoc comparisons were made within age and sex groups, there were no differences between PBS and □-syn pff injected mice. These results suggest marginal influence of □-syn pff injection at the post-surgical time points evaluated here (Figure S1 E and F). There were no significant main or interacting effects of injected material on speed on the 12 mm or 6 mm beam (Figure S1G and H). Motor impairment score, which indicates combined impairments in rotarod, wire hang, and horizontal beam tests, showed significant main effects of material ($F1,85 = 4.85$, $p = 0.030$) and material x sex interaction ($F1,85 = 5.68$, $p = 0.019$). Post-hoc tests revealed that this score was significantly impaired in aged male mice at 3 months post-pff injection ($p < 0.05$) (Fig. 2E and F). Together, aging increased □-syn pff associated pathology in the neocortex and limbic system resulting in more pronounced memory deficits as reflected by the fear conditioning test.

Enhanced infiltration of adaptive immune cells in aged mice inoculated with □-syn pff compared to young mice

We and others have shown [36,37] inflammatory responses involving T cells in mouse models of DLB/PD. To test the effects of aging on T cell infiltration in the □-syn pff model, we first performed immunohistochemistry with anti-CD3 antibody (T cell marker). We observed very few CD3 + cells in PBS-injected control mice of any age-group (Fig. 3A and C, E and G, left panels). However, young mice injected with □-syn pff showed a considerable infiltration by CD3 + cells in the neocortex, amygdala and striatum at 1-month after injection (Fig. 3A, right panel), that decreased at 3-month after injection (Fig. 3C, right

panel). These T cells were observed around blood vessels and in the interstitial space in the neuropil. Image analysis of CD3 + cell counts showed significant increase of CD3 + cells in neocortex, amygdala and striatum at 1-month post injection, and neocortex and striatum at 3-month post injection (Fig. 3B and D). In contrast, aged mice which were injected with □-syn pff showed considerably more robust infiltration by CD3 + cells at 1-month after injection (Fig. 3E right panel). Although the frequency of CD3 + cells was reduced at 3-months after injection (Fig. 3G right panel), the numbers remained above those seen in young mice. Image analysis of T cell showed significant increase in □-syn pff injected cohort compare to PBS injected cohort in all brain regions at both 1- and 3-month post injection (Fig. 3F and H). Comparison of CD3 + cell counts between young and aged mouse cohorts revealed that aged mice showed significantly higher CD3 + cell counts in the neocortex, amygdala and striatum at both 1- and 3-month after injection of □-syn pff (Figs. 3I-K).

To test if these CD3 + cells are T-helper cells or not, we next immunostained slides with an antibody against CD4. While the PBS injected young and aged mice displayed only a few CD4 + cells after injection (Figures S2A, C, E and G, left panels), remarkably, the □-syn pff injected young and aged mice at 1-month after injection showed several CD4 + cells in neocortex, amygdala and especially striatum (Figure S2A and E left panels), and these decreased at 3-month after injection (Figure S2C and G left panels). Image analysis of CD4 + cell counts between PBS and □-syn pff injected showed significant increase of CD4 + cells in □-syn pff injected cohorts of all brain regions inspected in both young and aged cohorts at 1- and 3-month after injection, except young mice cohort for the amygdala and striatum at 3-month after injection (Figure S2B, D, F and H). Comparison of CD4 + cell counts between young and aged mice cohorts at 1- and 3-month post injection showed greater CD4 + cells infiltration in the aged mice cohort, more prominent at 1-month after injection, with decreasing numbers 3-months after injection in both young and aged mice cohorts (Figure S2I-K). Together, these results show that aging promotes increased T cell (CD4) infiltration that accompanies □-syn pff spreading pathology.

Sustained presence of activated microglia in the CNS of aged mice injected with □-syn pff compared to young mice

As we and others have shown that innate cells play a role in the pathogenesis of PD in □-syn transgenic models [38,39], we investigated the contribution of aging on microglial and astroglial cells in the □-syn pff model. Immunohistochemical analysis with the Iba1 antibody showed highly branched and activated microglia in neocortex, amygdala and striatum of the □-syn pff injected in both young and aged mice cohorts (Fig. 4A, C, E and G, right panels) compared to PBS injected mice (Figs. 4A, C, E and G, left panels). Interestingly, differences between PBS and □-syn pff injected mice cohorts at 1 month returned to baseline at 3-month post injection (Figs. 4B, D, F and H). In contrast, comparison of Iba1 positive cells between young and aged mice cohorts showed greater numbers and level of activation of microglial cells in the aged mice cohort at 1- and 3-months post injection (Fig. 4I-K). In terms of GFAP positive astroglial cells, we observed significant astrogliosis in the neocortex, amygdala and striatum in the □-syn pff injected young and aged mice cohorts (Figure S3A, C, E and G right panels) compared to PBS injected young and aged mice cohorts (Figure S3A, C, E and G left panels) at both 1- and 3-months after injection

(Figure S3B, D, F and H). Image analysis of GFAP positive astroglial cells between young and aged mice cohorts (PBS and □-syn) mostly showed no differences between GFAP positive cells at 1- and 3-month after injection, only the neocortex of □-syn pff injected mice after 3 months showed increased in astrogliosis with aging (Figure S3I-K). We infer that sustained microglial activation contributes to neuropathy and behavioral deficits during □-syn induced disease progression in aged mice.

To investigate the relationship between the p-□-syn aggregates and the T and microglial cell infiltration, double immunolabeling studies with the antibodies against CD3 + or Iba1 and p-□-syn were performed in the young and aged mouse cohorts at 1 and 3 months after injection (Fig. 5A and 5G). In the young mice, the CD3 + cells were usually far from the □-syn aggregates in the neocortex, with closer proximity in the amygdala and striatum at 1- and 3-months post injection (Figs. 5B and C). However, in the aged mice there was closer proximity between p-□-syn neuropil threads and CD3 + cells in all the amygdala and striatum at 1 month (Fig. 5B) and all three regions of the brain analyzed at 3 months (Fig. 5C), direct comparison between young and aged mice confirmed the increased closer localization between T cells and p-□-syn aggregates in the aged mice in all 3 regions (Figs. 5D-F). Overall, compared to the T cells (Fig. 5A) the microglial cells and their processes were usually in closer proximity to the □-syn aggregates (Fig. 5G). In the young mice, the microglial cells were at some proximity to the □-syn aggregates in the neocortex, with closer proximity in the amygdala and striatum at 1- and 3-months post injection (Figs. 5H and I). However, in the aged mice there was greater proximity between p-□-syn aggregates and microglial cells with their processes surrounding the □-syn positive cells in all brain regions at 1 month (Fig. 5H) and in the neocortex and amygdala at 3 months (Fig. 5I). Direct comparison between young and aged mice confirmed the greater proximity between microglial cells and □-syn aggregates in the aged mice (Figs. 5J-L). Taken together these studies support the notion that microglial cells might be interacting □-syn aggregates during aging.

Transcriptomic analysis shows enhanced inflammation in the □-syn pff injected brains in aged mice compared to young mice

To characterize the molecular link between aging and □-syn pff-induced microglial activation we assayed the transcriptomes of purified microglia isolated from PBS and □-syn pff injected mice from young and aged mice. We found that the first principal component clearly distinguished gene expression profiles in cells from young and aged mice (Figure S4A). We first examined the effects of age by comparing PBS injected samples using DESeq2 and adjusting for multiple testing with Benjamini-Hochberg (BH) approach (adjusted p-value < 0.1). We identified 622 genes that were up-regulated (fold change > 2) (154 ≥ 4-fold genes shown for visualization purpose) and 188 genes that were down-regulated (fold change > 2) with age ($p < 0.05$) (Fig. 6A). That PC1 had a strong aging component was further substantiated by comparing age-associated differentially expressed genes (DEG_{age}) with the top 1000 PC1 genes identified by lasso regression (Figure S4B). We found that approximately 30% of DEG_{age} genes were in this group (gene set overlap p value 5.8e-51, including *C3*, *Il1rn*, *Olr1*, *Rxrg*, *Fam71a* and *Plk5* (highlighted in Figure S4B). Ingenuity Pathway Analysis (IPA) showed that DEG_{age} were enriched for inflammatory and immune system-associated pathways like ‘Communication with innate and adaptive immune cells’, ‘Altered T and

B cell signaling in Rheumatoid Arthritis' or pathways linked to IL-12 signaling while well-known upstream regulators of inflammation such as lipopolysaccharide (LPS), TNF, IL-1b and IL-6 were also implicated (Fig. 6B and Figure S5A). One of the upstream regulators, IL10RA which is a part of IL10 mediated anti-inflammatory cellular response, is highly repressed (right, Fig. 6B). A network constructed from pathways with more than 5 common enriched genes (or other molecules) that change with age highlighted inflammation and immune system-associated pathways like 'Communication with innate and adaptive immune cells', 'Altered T and B cell signaling in Rheumatoid Arthritis' or pathways linked to IL-12 signaling were linked (Fig. 6C). Based on the transcriptional upstream regulators projected from IPA, a network of the top upstream regulators (CSF2, LPS, TNF and poly rI:rC-RNA) and their target genes (or other molecules) was constructed (Fig. 6D). This showed that many age-associated genes had cytokines like CSF2 and TNF or molecules like LPS that mimic cytokine-related inflammatory responses, as common upstream transcriptional regulators which imply that the age-associated genes were related to inflammatory response. Cumulatively, these observations support the notion of accentuated inflammatory phenotype of microglia from aged mice. While age-associated inflammation has been reported in many mouse tissues including microglia [40–42], our gene set included many hitherto unknown genes and provide the baseline for evaluating the effects of -syn pff injection. A subset of genes dysregulated by age, as observed by RNA-Seq, were validated by quantitative RT-PCR (Figure S5B-C).

We next identified genes that were differentially expressed in response to -syn pff injection in young and aged mice (Fig. 7A). Analyses of these gene lists revealed several interesting features. First, -syn pff induced distinct responses in microglia from young and aged mice. Gene ontology analyses of upregulated genes using ToppGene [43] showed that 'Regulation of immune processes' was the only pathway (amongst the top 3) that was shared between the young and aged cohorts at the 1-month post injection. Similarly, 'neurogenesis' and 'neuronal development' pathways were the only ones amongst down-regulated genes that were common to both young and aged mice, respectively, at 1 month after injection. Second, beyond the small overlap at 1 month, gene expression trajectories in young and aged microglia diverged considerably. Most strikingly, whereas responses in young mice evolved to a robust 'myeloid activation' phenotype at 3 months after -syn pff injection, those in aged mice were dominated by pathways associated with cell death ('positive regulation of cell death' and 'response to glucocorticoids') and dysregulated proteostasis ('de novo protein folding' and 'establishment of protein localization') (Fig. 7A, detailed pathway results in Figure S6A). A subset of genes dysregulated by age or -syn pff challenge, as observed by RNA-Seq, were validated by quantitative RT-PCR (Fig. 7B). 30–50% of the genes dysregulated by 3 months of -syn pff treatment in aged mice changed in the same direction in an independent cohort of aged mice, however these trends didn't reach significance ($p < 0.05$) (data not shown). Genes that changed in response to -syn pff injection ($\geq$ 1.5-fold, $p \leq 0.01$) were processed through IPA to identify general features of these responses. We found that top canonical pathways were associated with neuronal system, neuroinflammation and leucocyte signaling (highlighted in yellow) which were uniformly repressed across the four groups (left, Figure S6B). Most upstream transcriptional regulators of DEGs behaved uniformly across all the groups (center) and similar results were found for the functions and diseases (right, Figure S6B).

Third, a significant proportion of gene expression changes induced by α-syn pff ($p < 0.05$) in young mice coincided with those that occurred with age ($p < 0.05$). Specifically, about a third of the genes that were up- or down-regulated by α-syn pff 1-month post injection changed in the same direction with age (Fig. 7C). At 3 months after α-syn pff injection almost half the pff-induced genes in young mice coincided with genes that were up-regulated by age alone, suggesting that pff continued to induce an aging phenotype up to 3 months after injection in young mice. By contrast, α-syn pff injection in aged mice induced age-associated genes strongly only at the 1-month post injection (Fig. 7C). A subset of genes dysregulated by both age and α-syn pff injection, as observed by RNA-Seq, were validated by quantitative RT-PCR (Figure S6C). Many genes induced by α-syn pff or by aging alone were classified as inflammation-associated in the MouseMine database [44](Figure S6D). We infer that α-syn pff injection induces a sustained aging-related microglial phenotype in young mice.

Discussion

The present study showed that aging resulted in more extensive accumulation of α-syn, greater infiltration of T cells and microgliosis and behavioral deficits. Distinctive inflammatory transcriptomic patterns in microglia showed that α-syn pff-induced genes networks in young mice (eg: LPS, TNFα, IL1b, IL6) that overlapped with genes differentially expressed in microglia in the aged mice (Figure S7). Moreover, based on the IPA, a network including CSF2, LPS, TNFα and poly rI:rC-RNA were indentified as top upstream regulators. We infer that the persistent α-syn pff challenge initially induces an aging phenotype that is followed by a distinct and presumably more deleterious gene expression program. This transition occurs between 1 and 3 months after α-syn pff injection in aged mice but not for at least 3 months after α-syn pff injection in young mice. Interestingly, α-syn pff did not down-regulate age-associated genes in aged mice even at the 1-month post injection, suggesting that aging had already conferred an early α-syn pff-like phenotype with respect to this subset of genes.

These results are consistent with the concept that α-syn aggregates might lead to neurodegeneration by dysregulating adaptive and innate immune responses [22–24, 45] and that aging plays an important role in this process. For example, recent studies have shown that intra-striatal injection of α-syn pff resulted in activation of microglia and astrocytes and infiltration of B, CD4 + T, CD8 + T, and natural killer cells in the brain at 5 months p.i., moreover in this study the authors showed alterations in the frequency and number of lymphoid cell subsets in the spleen and lymph nodes with minimum alterations in the blood [46]. In addition, a similar study in the Sprague Dawley rats demonstrated that intra-striatal injection of α-syn pff triggered MHCII-expressing cells are composed of both resident microglia as well as cells from the periphery that included monocytes/macrophages, and T cells [47]. Our study is different in that while previous studies were conducted in young rodents (2–3 months of age) and analysis was performed in the case of the mice at 5 months p.i. and in for the rats after 1, 3 and 6 months p.i., in the present study the focus was to investigate the effects of aging (18–19 momths old) on immune responses mediated by extracellular α-syn. Interestingly, in support of our findings a recent study showed that inoculation of α-syn

fibrils in the gut of aged (but not in the young) mice resulted in □-syn pathology in the midbrain accompanied by motor deficits [48].

The mechanisms through which aging might contribute to the more severe T cell infiltration, microglial-inflammatory responses and □-syn accumulation are not completely understood. However, our transcriptomic and pathway analysis showing that in the young mice □-syn pff triggered inflammatory networks similar to those observed in microglia from aged mice suggests complementary effects of aging and □-syn aggregates. In fact, age-associated increase in chronic, low-grade sterile inflammation has been termed “inflammaging” [11] which is strongly associated with age-associated disorders including AD, DLB, PD and other neurodegenerative disorders. Moreover, during aging, there is senescence of T cell populations. This includes reduced production of naïve T cells and accumulation of highly differentiated T cells resulting in a diminished T cell receptor repertoire [49].

In agreement with studies showing T cell infiltration following □-syn pff in rodent models [46,47], recent studies have shown that in DLB [36] and PD [50,51] there is abundant T cell infiltration in the brain. Likewise, studies in □-syn over-expressing mice that mimics DLB/PD [36] and multiple system atrophy [52] and neurotoxic models (MPTP challenge) in mice [53] and non-human primates [54] have reported extensive T cell infiltration in the CNS accompanied by microglial activation. Interestingly, alternative models where □-syn pff was administered systemically [22] or intra-enteric targeting of the ganglionic plexus have also shown dysregulation of immune responses with trafficking of lymphocytes, monocytes and macrophages into the CNS. Interestingly, depleting selected T-cell populations ameliorates dopaminergic neurodegeneration in animal models of PD, thus indicating a key role of adaptive immunity in the neurodegenerative process [45].

The molecular mechanisms through which age-related alterations in innate immune responses might be involved in synucleinopathies has recently gained interest [24,50]. Here based on the transcriptomics analysis projected from IPA, we found a network that included CSF2, LPS, TNF□ and poly rI:rC-RNA as common upstream transcriptional regulators. Interestingly, these pathways have a number of commonalities, including involvement in cytokine driven neuroinflammatory process, signaling via toll-like receptors (TLR’s) and regulation of microglial function. For example, CSF2 (also known as granulocyte macrophage stimulating factor [GM-CSF]) which is a cytokine that controls the production, differentiation, and function of granulocytes and macrophages in the CNS promotes microglia activation and inflammation [55]. In individuals with a rare kind of dementia with demyelination known as adult-onset leukoencephalopathy with axonal spheroids and pigmented glia (ALSP); CSF2 is increased and colony stimulating factor 1 receptor (CSF-1R) is haploinsufficient [56]. Remarkably, a recent study showed that downregulation of CSF2 in CSF-1R deficient mice rescues the behavioral and neuropathological alterations in the mouse model of ALSP indicating that CSF2 is critical in regulating microglial function and inflammation in the CNS and has been proposed as a therapeutical target for ALSP [57]. Until this study, the role of CSF2 in PD/DLB and other neurodegenerative disorders have not been considered, however increased levels of CSF-R1 have been described in AD and inhibitors of CSF-R1 have been

proposed as a therapy for PD and other neurodegenerative disorders [58]. In contrast, in recent years, the role of TLR's in DLB/PD has been extensive considered [59] and TLR2 has been shown to be a key mediator of the neurotoxic and pro-inflammatory effects of extracellular □-syn aggregates [26]. Taken together our network analysis showed that pathways involving stimulation of microglia via TLR's and CSF-R are critical toward understanding the role of aging in DLB/PD (Figure S7).

In conclusion the present study showed that aging triggered a more inflamed micro-environment in the □-syn pff model of DLB/PD, resulting in increase T cell infiltration and microgliosis. Microglia displayed distinctive inflammatory transcriptomic patterns overlapping with genes differentially expressed in microglia in the aged mice. These results point to the possibility that targeting selected neuro-immune responses involving CSF-R and TLR's might be important in developing treatments for DLB/PD.

Methods

Animals

A total of 66 both male and female C57BL/6 wild type mice were used in this study. The "young" group were purchased from Charles River at the age of 3-4 months old (n=31), and the "aged" group were provided by the NIA funded rodent colonies [also derived from the Charles River derived strains] at the age of 18-19 months old (n=35) (Table 1). All experiments were performed in accordance with the ALAC-and ACUC approved protocols of NIA/NIH.

Stereotaxic surgery and study design

After deeply anesthetizing mice with isoflurane, the animals were immobilized in a stereotaxic frame and bilateral stereotaxic injections were made using predetermined coordinates in the striatum (bregma, 0.2 mm; lateral, 2 mm; and depth, 3.2 mm) with Hamilton syringe under aseptic conditions. All animals were observed during and after surgery, and pain killer was administered for 3 days including surgery day. One-half the number of mice in each group were injected 5 mg (2.5 ml of 2 mg/ml concentration) of □-syn pff (generous gift from Dr. Kelvin Luk at University of Pennsylvania, CNDR) [60] and the other half were injected 2.5 ml of PBS as a control. For each group (young and aged) mice were analyzed at 1- and 3-months after the injection with attention to sex balance. The experiment in the aged mice was repeated with an addition set of mice (n=38)

Behavioral Testing

Open field test: Mice were placed in a 40 cm x 40 cm x 40 cm white plexiglass chamber (Maze Engineers; Boston, MA) under dim lighting and recorded for 15 minutes. Behavior was analyzed with ANY-Maze software (Stoelting; Wood Dale, IL). Behavior from the first 3 minutes was found to be most affected by □-syn pff injection, so all analysis was conducted during this time period.

Fear conditioning: Mice were placed in a rectangular conditioning chamber (Med Associates) with metal bars for a floor and lit by dim white light. After a 2-minutes acclimation period, mice were presented with a 30-second tone that co-terminated with a 2-second, 0.5mA scrambled shock with alternating current. A second tone-shock pairing was delivered 60 seconds later, and mice remained in the chamber an additional two minutes. The following day mice were placed in the chamber for 5 minutes to assess freezing conditioned to the context. On day 3 the chamber was altered with insertion of a smooth plastic floor, black triangular wall inset, and illumination only by infrared lighting. Mint odor (McCormick; Hunt Valley, MD) was applied to the ceiling of the chamber to further differentiate it from the previous context. Mice were placed in the modified chamber for a 2-minute baseline, and then a constant tone was played for 3 minutes. All freezing was recorded with a side-mounted camera and scored using automated software with default settings for freezing thresholds.

Wire hang: Mice were placed on a wire cage-top that was inverted to allow mice to hang upside down while grasping all four limbs. Latency to fall was recorded up to a maximum of 600 seconds. Three trials were conducted with at least 30 minutes between trials. Log_{10} transformation on fall latencies was required to produce a normal distribution.

Rotarod: Mice were tested in eight trials on a 3.2cm diameter drum (Med-Associates; St Albans, VT) that accelerated from 4 to 40 rpm over 300 seconds. On the first two days mice were tested in one and then two trials, respectively. On these days latency until the first fall was recorded, but mice were replaced on the rod after the first trial. On the third day mice underwent five consecutive trials in which they were removed from the apparatus after the first fall. Each trial was separated by at least 30 minutes. Latency to fall (max 300s) was analyzed; mice approached maximal performance in the last 3 trials; therefore averages from all trials preceding those were averaged into a single value.

Elevated zero maze: Mice were tested for five minutes in a zero maze apparatus elevated 61cm above the floor. The floor of the apparatus was a gray plexiglass 5cm-wide circular track with 50cm outer diameter. Two opposite quadrants had 20cm tall black walls, and the quadrants in between had a 0.5cm tall lip to contain mice. Video was analyzed with Noldus Ethovision (Wageningen, Netherlands).

Horizontal beam: On the first day mice were trained to run down a series of 1-meter long rectangular plexiglass beams (24, 12, and 6mm in diameter) towards a 20 x 20 x 20cm dark goal box. The room was brightly lit, and beams were suspended 50cm above the floor with a vinyl net to catch any mice that might fall. On the second day trials were recorded with an overhead camera as mice ran two trials each on the 12 and 6mm beams. Speed in the middle 60cm of the beam was recorded and analyzed with ANY-Maze software. Data from trials on similar beam widths were averaged.

Primary microglia preparation

Primary microglia were isolated from the mice brains utilizing Adult Brain Dissociation Kit (Miltenyi Biotec, Auburn, CA) according to the manufacturer's instruction. Briefly, enzyme-mixed mice brains were dissociated by gentleMACS Octo Dissociator with Heaters (Miltenyi Biotec) for 30 minutes. After a

filtration with strainer, the brain homogenates were incubated with CD11b magnetic beads (Miltenyi Biotec) for 15 minutes. The incubated beads were rinsed 3 times with MACS buffer (Miltenyi Biotec) before eluting the cells.

Bulk RNA-Seq library preparation

RNA quality was assessed by using Agilent RNA 6000 Nano Kit and Agilent 2100 Bioanalyzer according to the manufacturer's instructions. Qualified total RNA (RIN > 8, 10 ng) from each sample was processed by following SMARTer® Stranded Total RNA-Seq Kit v2 - Pico Input Mammalian protocol (Takara Bio USA, Inc., CA). Briefly, total RNA was converted to cDNA followed by addition of barcodes and adapters. The library was purified using AMPure beads. Takara Bio's SMART (Switching Mechanism at the 5' end of RNA Template) technology was used to remove ribosomal cDNA. After final library PCR amplification and cleaning, the libraries were quantified on the Agilent 2100 Bioanalyzer using the Agilent High Sensitivity DNA Kit. The libraries were the sequenced at single end with read length of 75 bp on Illumina HiSeq 4000 platform at the Johns Hopkins Sequencing Core facility (Baltimore, MD) to yield an average depth of 70 million reads per sample.

Bulk RNA-Seq data analysis

RNA-Seq 75bp single-end reads were analyzed with kallisto-v0.46.2, using mm10; Ensembl v96 annotation. From the Bioanalyzer results, we calculated an average fragment size of 250bp -after subtracting 120bp for the adapter size and mean standard deviation ~ 80 [kallisto parameters for single-end: -l 250 -s 80]. We aggregated to gene level by applying *tximport* to *kallisto* TPM counts and identified covariates to exclude from the analysis by principal component analysis (R package prcomp). From the top 1000 most variable genes of age principal component (PC1), we identified the most variable genes with aging by applying elastic net regression (*glmnet*). Differential expression analysis for studying age effect and PFF effect respectively was performed with *DESeq2*; and applied *Benjamini Hochberg* multiple test correction. We identified up- and down-regulated genes with at least 2-fold change at p-value$\leq$0.05. All overlap significance p-values were calculated by hypergeometric tests. IPA was used to identify enriched canonical pathways, upstream regulators and enriched functions and diseases.

Neuropathology, immunohistochemistry and image analysis

At one- or three-months post-injection, all injected mice were deeply anesthetized and transcardially perfused with 30 ml of PBS. A hemisphere from each of harvested brains were first fixed in 70 % Ethanol in PBS and then embedded in paraffin. Then 6µm-thick sections were cut through the entire CNS for conventional neuropathological examination and immunohistochemistry (IHC). Sections were incubated overnight at 4^{o}C with the following primary antibodies: 81A (anti-□-syn, p-S129, gift from Drs. Virginia Lee and John Trojanowski at University of Pennsylvania, CNDR, mouse, 1:20K, citrate buffer treatment), CD3 (abcam ab16669, or Thermo Fisher Scientific MA5-14524 rabbit polyclonal, 1:200, citrate buffer treatment), CD4 (abcam ab183685, rabbit polyclonal, 1:1000, tris buffer treatment), GFAP (Millipore MAB3402, mouse monoclonal, 1:200) and Iba1 (microglia marker, abcam AB178846, rabbit polyclonal,

citrate buffer treatment). Sections were then incubated in biotin-tagged anti-mouse or anti-rabbit IgG1 (1:400, Vector Lab) secondary antibodies, followed by Avidin DHRP (1:200, ABC Elite, Vector Lab), visualized with diaminobenzidine (DAB, Vector Lab), counterstained with hematoxylin, coverslipped and imaged with a Zeiss wide field microscope. For the double immunofluorescent, brain sections were incubated with a combination of antibodies against □-syn, p-S129 and T cell marker (81A/CD3) or p-S129 and Iba1 marker (p-S129/Iba1). Sections were labeled with FITC-tagged and Texas-red secondary antibodies, nuclei are stained with DAPI (Hoechst 33258, Thermo Fisher H3569, 1:100,000), reduced background with TrueBlackTM Lipofuscin Autofluorescence Quencher (Biotium: 23007) diluted 1/40 in 70% EtOH and mounted under glass coverslips with anti-fading media (ProLong™ Gold Antifade Mountant, Thermo Fisher Scientific). Briefly as previously described [36], all sections were processed and imaged under the same standardized conditions and blind coded. Four fields from the frontal cortex, amygdala and striatum were examined for each section and performed in duplicate for each mouse. Sections visualized with DAB were imaged with an Olympus BX41 microscope and analyzed with the Image Quant 1.43 program (NIH) to determine the number of CD3+, CD4+, GFAP+, and Iba1+ cells per field (230 mm x 184 mm). Double immunolabeled sections were imaged with an Apotome II mounted in a Carl Zeiss AxioImager Z1 microscope. Optical sections (0.5 mm thick) were analyzed via the Zen 2.3 platform to determine the average number of CD3 cells, in close proximity to □-syn+ neuritic process.

Statistical analysis

Values shown in the figures are presented as mean ± SEM. Behavioral results were initially analyzed by analysis of variance of a linear model with interacting terms for age, sex, material, and interval, with an additional factor to account for batch variability. Due to the extensive number of terms in these models, only the most pertinent results are reported. Dunnett's post-hoc tests were used to compare pff-injected mice vs relevant PBS-injected controls. "Motor impairment score" was derived from speed on the 12mm-wide horizontal beam, rotarod, and wire hang. Data for each individual test were first converted to z-scores within each age- and sex-matched group of animals and then averaged and multiplied by -1. For neuropathological analysis, P values for determination of statistical significance of the differences were calculated with the one-way, two-way ANOVA and unpaired Student's *t* test

Declarations

Acknowledgments

The authors wish to thank Dr. Kevin Luk at University of Pennsylvania for kindly providing the □-syn pff preparations, and Dr. Zu-Xi Yu at the Pathology Facility in the National Heart, Lung, and Blood Institute (NHLBI) to allow us to use paraffin processor and embedding center. This work was supported by NIA/NIH intramural research program grant 1ZIAAG000936-03 (to J.M.S., R.S., and E.M.)

References

1 Hou, Y. *et al.* Ageing as a risk factor for neurodegenerative disease. *Nat Rev Neurol* **15**, 565-581, doi:10.1038/s41582-019-0244-7 (2019).

2 Goedert, M. Alpha-synuclein and neurodegenerative diseases. *Nat Rev Neurosci* **2**, 492-501, doi:10.1038/35081564 (2001).

3 Kotzbauer, P. T., Trojanowsk, J. Q. & Lee, V. M. Lewy body pathology in Alzheimer's disease. *J Mol Neurosci* **17**, 225-232, doi:10.1385/jmn:17:2:225 (2001).

4 Twohig, D. & Nielsen, H. M. α-synuclein in the pathophysiology of Alzheimer's disease. *Mol Neurodegener* **14**, 23, doi:10.1186/s13024-019-0320-x (2019).

5 Alafuzoff, I. & Hartikainen, P. Alpha-synucleinopathies. *Handb Clin Neurol* **145**, 339-353, doi:10.1016/b978-0-12-802395-2.00024-9 (2017).

6 Savica, R., Boeve, B. F. & Mielke, M. M. When Do α-Synucleinopathies Start? An Epidemiological Timeline: A Review. *JAMA Neurol* **75**, 503-509, doi:10.1001/jamaneurol.2017.4243 (2018).

7 Walker, L. *et al.* Neuropathologically mixed Alzheimer's and Lewy body disease: burden of pathological protein aggregates differs between clinical phenotypes. *Acta Neuropathol* **129**, 729-748, doi:10.1007/s00401-015-1406-3 (2015).

8 Coughlin, D. G. *et al.* Hippocampal subfield pathologic burden in Lewy body diseases vs. Alzheimer's disease. *Neuropathol Appl Neurobiol*, doi:10.1111/nan.12659 (2020).

9 Ferman, T. J. *et al.* The limbic and neocortical contribution of alpha-synuclein, tau, and amyloid beta to disease duration in dementia with Lewy bodies. *Alzheimers Dement* **14**, 330-339, doi:10.1016/j.jalz.2017.09.014 (2018).

10 Ferrucci, L. *et al.* Measuring biological aging in humans: A quest. *Aging Cell* **19**, e13080, doi:10.1111/acel.13080 (2020).

11 Royce, G. H., Brown-Borg, H. M. & Deepa, S. S. The potential role of necroptosis in inflammaging and aging. *Geroscience* **41**, 795-811, doi:10.1007/s11357-019-00131-w (2019).

12 López-Otín, C., Blasco, M. A., Partridge, L., Serrano, M. & Kroemer, G. The hallmarks of aging. *Cell* **153**, 1194-1217, doi:10.1016/j.cell.2013.05.039 (2013).

13 Saez-Atienzar, S. & Masliah, E. Cellular senescence and Alzheimer disease: the egg and the chicken scenario. *Nat Rev Neurosci* **21**, 433-444, doi:10.1038/s41583-020-0325-z (2020).

14 Hipp, M. S., Kasturi, P. & Hartl, F. U. The proteostasis network and its decline in ageing. *Nat Rev Mol Cell Biol* **20**, 421-435, doi:10.1038/s41580-019-0101-y (2019).

15 Scott, D. A. *et al.* A pathologic cascade leading to synaptic dysfunction in alpha-synuclein-induced neurodegeneration. *J Neurosci* **30**, 8083-8095, doi:10.1523/jneurosci.1091-10.2010 (2010).

16 Lee, S. J., Desplats, P., Sigurdson, C., Tsigelny, I. & Masliah, E. Cell-to-cell transmission of non-prion protein aggregates. *Nat Rev Neurol* **6**, 702-706, doi:10.1038/nrneurol.2010.145 (2010).

17 Desplats, P. *et al.* Inclusion formation and neuronal cell death through neuron-to-neuron transmission of alpha-synuclein. *Proc Natl Acad Sci U S A* **106**, 13010-13015, doi:10.1073/pnas.0903691106 (2009).

18 Thakur, P. *et al.* Modeling Parkinson's disease pathology by combination of fibril seeds and α-synuclein overexpression in the rat brain. *Proc Natl Acad Sci U S A* **114**, E8284-e8293, doi:10.1073/pnas.1710442114 (2017).

19 Luk, K. C. *et al.* Pathological α-synuclein transmission initiates Parkinson-like neurodegeneration in nontransgenic mice. *Science* **338**, 949-953, doi:10.1126/science.1227157 (2012).

20 Lee, H. J., Bae, E. J. & Lee, S. J. Extracellular α--synuclein-a novel and crucial factor in Lewy body diseases. *Nat Rev Neurol* **10**, 92-98, doi:10.1038/nrneurol.2013.275 (2014).

21 Van der Perren, A. *et al.* The structural differences between patient-derived alpha-synuclein strains dictate characteristics of Parkinson's disease, multiple system atrophy and dementia with Lewy bodies. *Acta Neuropathol* **139**, 977-1000, doi:10.1007/s00401-020-02157-3 (2020).

22 Peralta Ramos, J. M. *et al.* Peripheral Inflammation Regulates CNS Immune Surveillance Through the Recruitment of Inflammatory Monocytes Upon Systemic α-Synuclein Administration. *Front Immunol* **10**, 80, doi:10.3389/fimmu.2019.00080 (2019).

23 Surendranathan, A., Rowe, J. B. & O'Brien, J. T. Neuroinflammation in Lewy body dementia. *Parkinsonism Relat Disord* **21**, 1398-1406, doi:10.1016/j.parkreldis.2015.10.009 (2015).

24 Allen Reish, H. E. & Standaert, D. G. Role of α-synuclein in inducing innate and adaptive immunity in Parkinson disease. *J Parkinsons Dis* **5**, 1-19, doi:10.3233/jpd-140491 (2015).

25 Gelders, G., Baekelandt, V. & Van der Perren, A. Linking Neuroinflammation and Neurodegeneration in Parkinson's Disease. *J Immunol Res* **2018**, 4784268, doi:10.1155/2018/4784268 (2018).

26 Kim, C. *et al.* Neuron-released oligomeric α-synuclein is an endogenous agonist of TLR2 for paracrine activation of microglia. *Nat Commun* **4**, 1562, doi:10.1038/ncomms2534 (2013).

27 Lee, H. J. *et al.* Direct transfer of alpha-synuclein from neuron to astroglia causes inflammatory responses in synucleinopathies. *J Biol Chem* **285**, 9262-9272, doi:10.1074/jbc.M109.081125 (2010).

28 Grozdanov, V. *et al.* Increased Immune Activation by Pathologic α-Synuclein in Parkinson's Disease. *Ann Neurol* **86**, 593-606, doi:10.1002/ana.25557 (2019).

29 Hughes, C. D. *et al.* Picomolar concentrations of oligomeric alpha-synuclein sensitizes TLR4 to play an initiating role in Parkinson's disease pathogenesis. *Acta Neuropathol* **137**, 103-120, doi:10.1007/s00401-018-1907-y (2019).

30 Kim, C. *et al.* Immunotherapy targeting toll-like receptor 2 alleviates neurodegeneration in models of synucleinopathy by modulating α-synuclein transmission and neuroinflammation. *Mol Neurodegener* **13**, 43, doi:10.1186/s13024-018-0276-2 (2018).

31 Caplan, I. F. & Maguire-Zeiss, K. A. Toll-Like Receptor 2 Signaling and Current Approaches for Therapeutic Modulation in Synucleinopathies. *Front Pharmacol* **9**, 417, doi:10.3389/fphar.2018.00417 (2018).

32 La Vitola, P. *et al.* Alpha-synuclein oligomers impair memory through glial cell activation and via Toll-like receptor 2. *Brain Behav Immun* **69**, 591-602, doi:10.1016/j.bbi.2018.02.012 (2018).

33 Dzamko, N. *et al.* Toll-like receptor 2 is increased in neurons in Parkinson's disease brain and may contribute to alpha-synuclein pathology. *Acta Neuropathol* **133**, 303-319, doi:10.1007/s00401-016-1648-8 (2017).

34 Galiano-Landeira, J., Torra, A., Vila, M. & Bove, J. CD8 T cell nigral infiltration precedes synucleinopathy in early stages of Parkinson's disease. *Brain*, doi:10.1093/brain/awaa269 (2020).

35 Lindestam Arlehamn, C. S., Garretti, F., Sulzer, D. & Sette, A. Roles for the adaptive immune system in Parkinson's and Alzheimer's diseases. *Curr Opin Immunol* **59**, 115-120, doi:10.1016/j.coi.2019.07.004 (2019).

36 Iba, M. *et al.* Neuroinflammation is associated with infiltration of T cells in Lewy body disease and alpha-synuclein transgenic models. *J Neuroinflammation* **17**, 214, doi:10.1186/s12974-020-01888-0 (2020).

37 Subbarayan, M. S., Hudson, C., Moss, L. D., Nash, K. R. & Bickford, P. C. T cell infiltration and upregulation of MHCII in microglia leads to accelerated neuronal loss in an alpha-synuclein rat model of Parkinson's disease. *J Neuroinflammation* **17**, 242, doi:10.1186/s12974-020-01911-4 (2020).

38 Watson, M. B. *et al.* Regionally-specific microglial activation in young mice over-expressing human wildtype alpha-synuclein. *Exp Neurol* **237**, 318-334, doi:10.1016/j.expneurol.2012.06.025 (2012).

39 Su, X. *et al.* Synuclein activates microglia in a model of Parkinson's disease. *Neurobiol Aging* **29**, 1690-1701, doi:10.1016/j.neurobiolaging.2007.04.006 (2008).

40 Olah, M. *et al.* A transcriptomic atlas of aged human microglia. *Nat Commun* **9**, 539, doi:10.1038/s41467-018-02926-5 (2018).

41 Schaum, N. *et al.* Ageing hallmarks exhibit organ-specific temporal signatures. *Nature* **583**, 596-602, doi:10.1038/s41586-020-2499-y (2020).

42 Ximerakis, M. *et al.* Single-cell transcriptomic profiling of the aging mouse brain. *Nat Neurosci* **22**, 1696-1708, doi:10.1038/s41593-019-0491-3 (2019).

43 Chen, J., Xu, H., Aronow, B. J. & Jegga, A. G. Improved human disease candidate gene prioritization using mouse phenotype. *BMC Bioinformatics* **8**, 392, doi:10.1186/1471-2105-8-392 (2007).

44 Motenko, H., Neuhauser, S. B., O'Keefe, M. & Richardson, J. E. MouseMine: a new data warehouse for MGI. *Mamm Genome* **26**, 325-330, doi:10.1007/s00335-015-9573-z (2015).

45 Campos-Acuña, J., Elgueta, D. & Pacheco, R. T-Cell-Driven Inflammation as a Mediator of the Gut-Brain Axis Involved in Parkinson's Disease. *Front Immunol* **10**, 239, doi:10.3389/fimmu.2019.00239 (2019).

46 Earls, R. H. *et al.* Intrastriatal injection of preformed alpha-synuclein fibrils alters central and peripheral immune cell profiles in non-transgenic mice. *J Neuroinflammation* **16**, 250, doi:10.1186/s12974-019-1636-8 (2019).

47 Harms, A. S. *et al.* α-Synuclein fibrils recruit peripheral immune cells in the rat brain prior to neurodegeneration. *Acta Neuropathol Commun* **5**, 85, doi:10.1186/s40478-017-0494-9 (2017).

48 Challis, C. *et al.* Gut-seeded alpha-synuclein fibrils promote gut dysfunction and brain pathology specifically in aged mice. *Nat Neurosci* **23**, 327-336, doi:10.1038/s41593-020-0589-7 (2020).

49 Pangrazzi, L. & Weinberger, B. T cells, aging and senescence. *Exp Gerontol* **134**, 110887, doi:10.1016/j.exger.2020.110887 (2020).

50 Chen, Z., Chen, S. & Liu, J. The role of T cells in the pathogenesis of Parkinson's disease. *Prog Neurobiol* **169**, 1-23, doi:10.1016/j.pneurobio.2018.08.002 (2018).

51 Lindestam Arlehamn, C. S. *et al.* α-Synuclein-specific T cell reactivity is associated with preclinical and early Parkinson's disease. *Nat Commun* **11**, 1875, doi:10.1038/s41467-020-15626-w (2020).

52 Williams, G. P. *et al.* T cell infiltration in both human multiple system atrophy and a novel mouse model of the disease. *Acta Neuropathol* **139**, 855-874, doi:10.1007/s00401-020-02126-w (2020).

53 Chandra, G., Roy, A., Rangasamy, S. B. & Pahan, K. Induction of Adaptive Immunity Leads to Nigrostriatal Disease Progression in MPTP Mouse Model of Parkinson's Disease. *J Immunol* **198**, 4312-4326, doi:10.4049/jimmunol.1700149 (2017).

54 Seo, J. *et al.* Chronic Infiltration of T Lymphocytes into the Brain in a Non-human Primate Model of Parkinson's Disease. *Neuroscience* **431**, 73-85, doi:10.1016/j.neuroscience.2020.01.043 (2020).

55 Dikmen, H. O. *et al.* GM-CSF induces noninflammatory proliferation of microglia and disturbs electrical neuronal network rhythms in situ. *J Neuroinflammation* **17**, 235, doi:10.1186/s12974-020-01903-4 (2020).

56 Chitu, V. *et al.* Phenotypic characterization of a Csf1r haploinsufficient mouse model of adult-onset leukodystrophy with axonal spheroids and pigmented glia (ALSP). *Neurobiol Dis* **74**, 219-228, doi:10.1016/j.nbd.2014.12.001 (2015).

57 Chitu, V. *et al.* Microglial Homeostasis Requires Balanced CSF-1/CSF-2 Receptor Signaling. *Cell Rep* **30**, 3004-3019 e3005, doi:10.1016/j.celrep.2020.02.028 (2020).

58 Walker, D. G., Tang, T. M. & Lue, L. F. Studies on Colony Stimulating Factor Receptor-1 and Ligands Colony Stimulating Factor-1 and Interleukin-34 in Alzheimer's Disease Brains and Human Microglia. *Front Aging Neurosci* **9**, 244, doi:10.3389/fnagi.2017.00244 (2017).

59 Beraud, D. & Maguire-Zeiss, K. A. Misfolded alpha-synuclein and Toll-like receptors: therapeutic targets for Parkinson's disease. *Parkinsonism Relat Disord* **18 Suppl 1**, S17-20, doi:10.1016/S1353-8020(11)70008-6 (2012).

60 Zhang, B. *et al.* Stereotaxic Targeting of Alpha-Synuclein Pathology in Mouse Brain Using Preformed Fibrils. *Methods Mol Biol* **1948**, 45-57, doi:10.1007/978-1-4939-9124-2_5 (2019).

Table

Table 1
Mouse numbers used in this experiment.

		Young		**Aged**			
				Cohort 1		Cohort 2	
		1 mo	3 mo	1 mo	3 mo	1 mo	3 mo
PBS	Male	4	4	5	4	5	5
	Female	4	4	3	4	5	3
□-syn pff	Male	3	4	5	5	5	4
	Female	4	4	5	4	5	5
	total	15	16	18	17	20	17

Figures

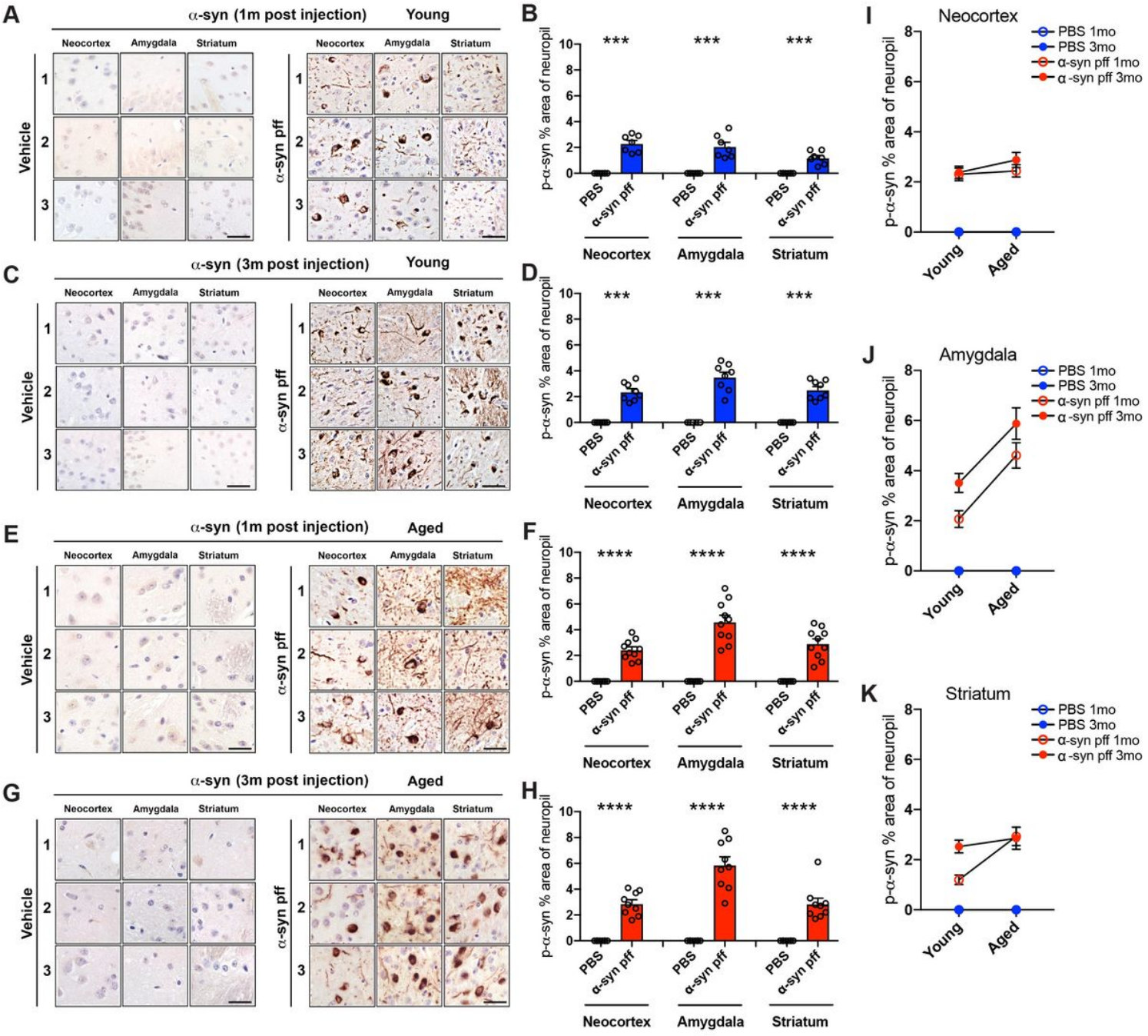

Figure 1

Immunohistochemical analysis for phosphorylated-α-syn (p-α-syn) in young and aged wt mice at 1- and 3-momth post-injection with PBS or α-syn pff. (A) Representative images of p-α-syn immunostaining in young mouse cohort at 1-month post injection. Images are from three different mice (1, 2 and 3) of three brain regions (cortex, amygdala, and striatum). Left panels are PBS (vehicle) injected and right are α-syn pff injected. (B) Image analysis of p-α-syn % area of neuropil of young mouse cohort at 1-month post

injection. (C) p-□-syn immunostaining of young mouse cohort at 3-month post injection. Same format as A. (D) Image analysis of p-□-syn % area of neuropil of young mouse cohort at 3-month post injection. (E) p-□-syn immunostaining of aged mouse cohort at 1-month post injection. Same format as A. (F) Image analysis of p-□-syn % area of neuropil of aged mouse cohort at 1-month post injection. (G) p-□-syn immunostaining of aged mouse cohort at 3-month post injection. Same format as A. (H) Image analysis of p-□-syn % area of neuropil of aged mouse cohort at 3-month post injection. (I-K) Comparison of image analysis of p-□-syn positive % area of neuropil in cortex (I), amygdala (J) and amygdala (K) of □-syn pff injected mice at 1- and 3-month post-injection in young (blue) and aged (red) mouse cohorts. Scale bar is 25 mm. ***p < 0.001; ****p < 0.0001

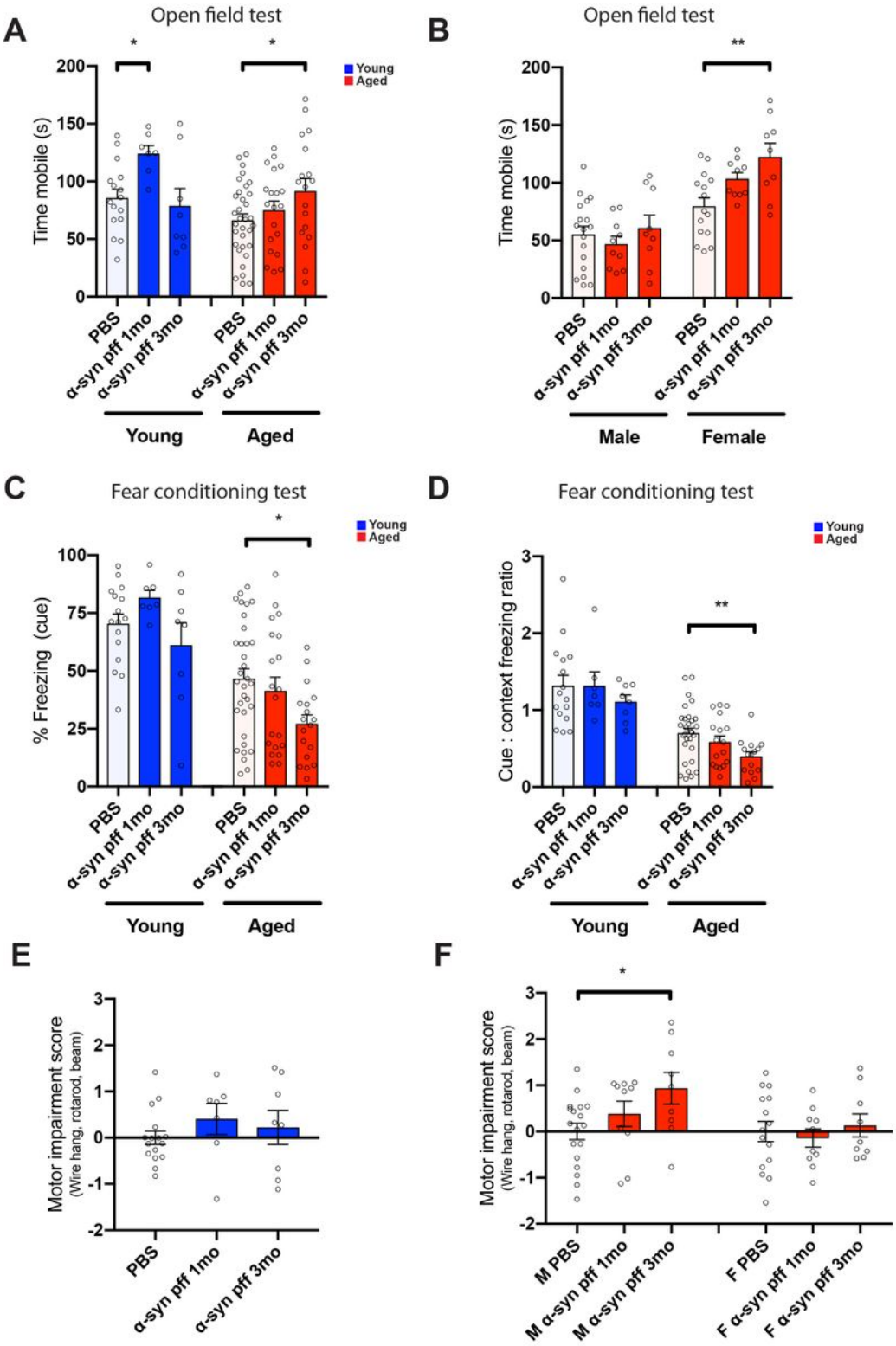

Figure 2

Behavioral analysis of young and aged wt mice at 1- and 3-momth post-injection with PBS or α-syn pff. (A) Time traveled (sec) for the first 3-minute bin in the open field test in young and aged mouse cohorts. (B) Time traveled (sec) for the first 3-minute bin in the open field test in the aged mouse cohorts separated by sex. (C) Percentage of freezing time to the cue freezing to the cue in the fear conditioning test. (D) The ratio of freezing to cue:context in the fear conditioning test. (E) Averaged scores from three

locomotor tests (wire hang, rota-rod and horizontal beam). (F) Each test was normalized by calculating how many standard deviations worse than age/sex-matched PBS controls in young and aged mouse cohorts. *p < 0.05; **p < 0.01

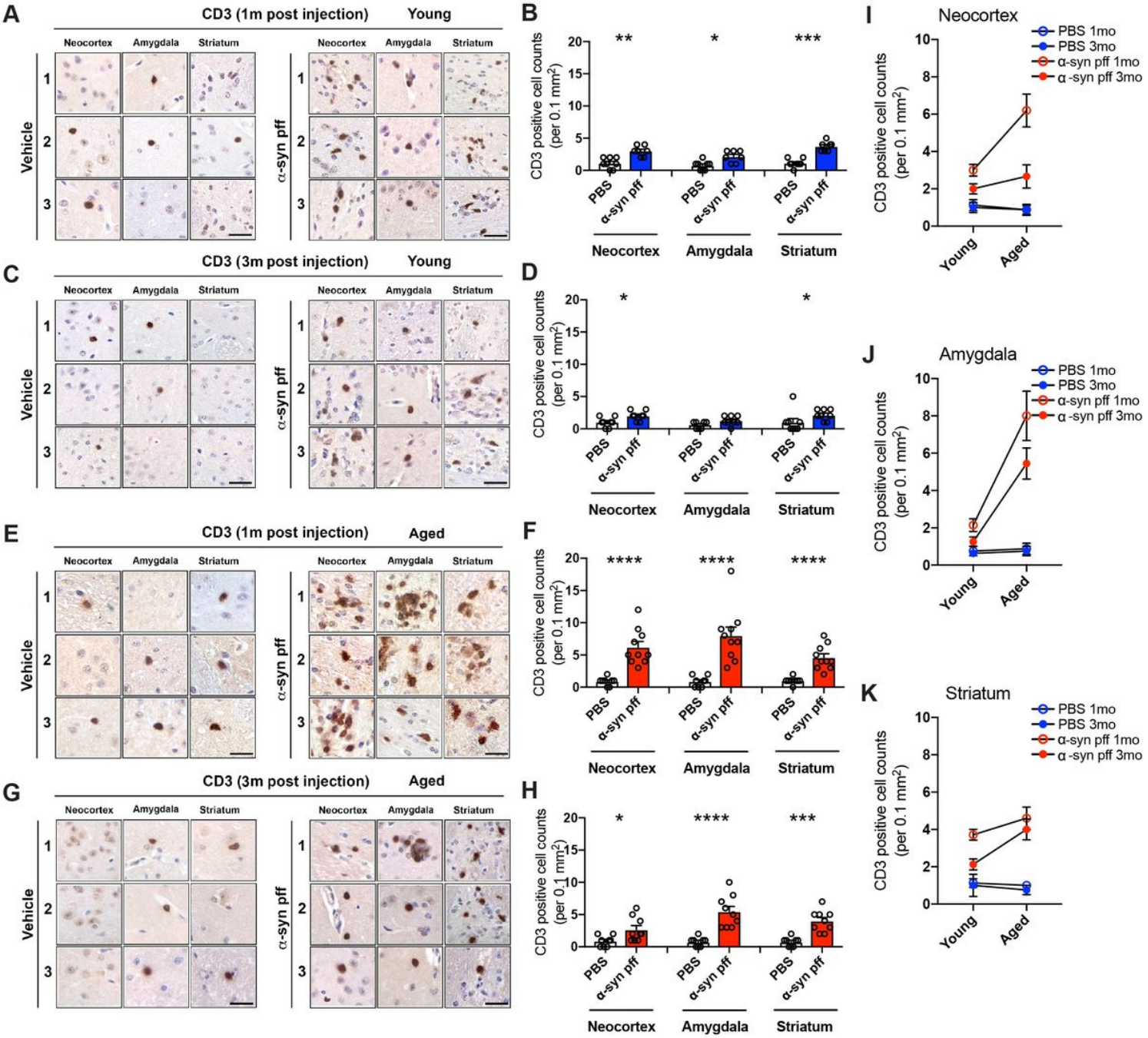

Figure 3

Immunohistochemical analysis of T cells with the CD3 antibody in young and aged wt mice at 1- and 3-month post-injection with PBS or □-syn pff. (A) CD3 immunostaining images of young mouse cohort at 1-month post injection. Images are from three different mice (1, 2 and 3) of three brain regions (cortex, amygdala, and striatum). Left panels are PBS (vehicle) injected and right are □-syn pff injected. (B) Image analysis of CD3 positive cell counts per 0.1mm2 of young mouse cohort at 1-month post injection. (C) CD3 immunostaining images of young mouse cohort at 3-month post injection. Same format as A. (D)

Image analysis of CD3 positive cell counts per 0.1mm2 of young mouse cohort at 3-month post injection. (E) CD3 immunostaining images of aged mouse cohort at 1-month post injection. Same format as A. (F) Quantitative analysis of CD3 positive cell counts per 0.1mm2 of aged mouse cohort at 1-month post injection. (G) CD3 immunostaining images of aged mouse cohort at 3-month post injection. Same format as A. (H) Image analysis of CD3 positive cell counts per 0.1mm2 of aged mouse cohort at 3-month post injection. (I-K) Comparison of image analysis of CD3 positive cell counts per 0.1mm2 in cortex (I), amygdala (J) and amygdala (K) of □-syn pff injected mice at 1- and 3-month post-injection in young (blue) and aged (red) mouse cohorts. Scale bar is 40 mm. *p < 0.05; **p < 0.01; ***p < 0.001; ****p < 0.0001

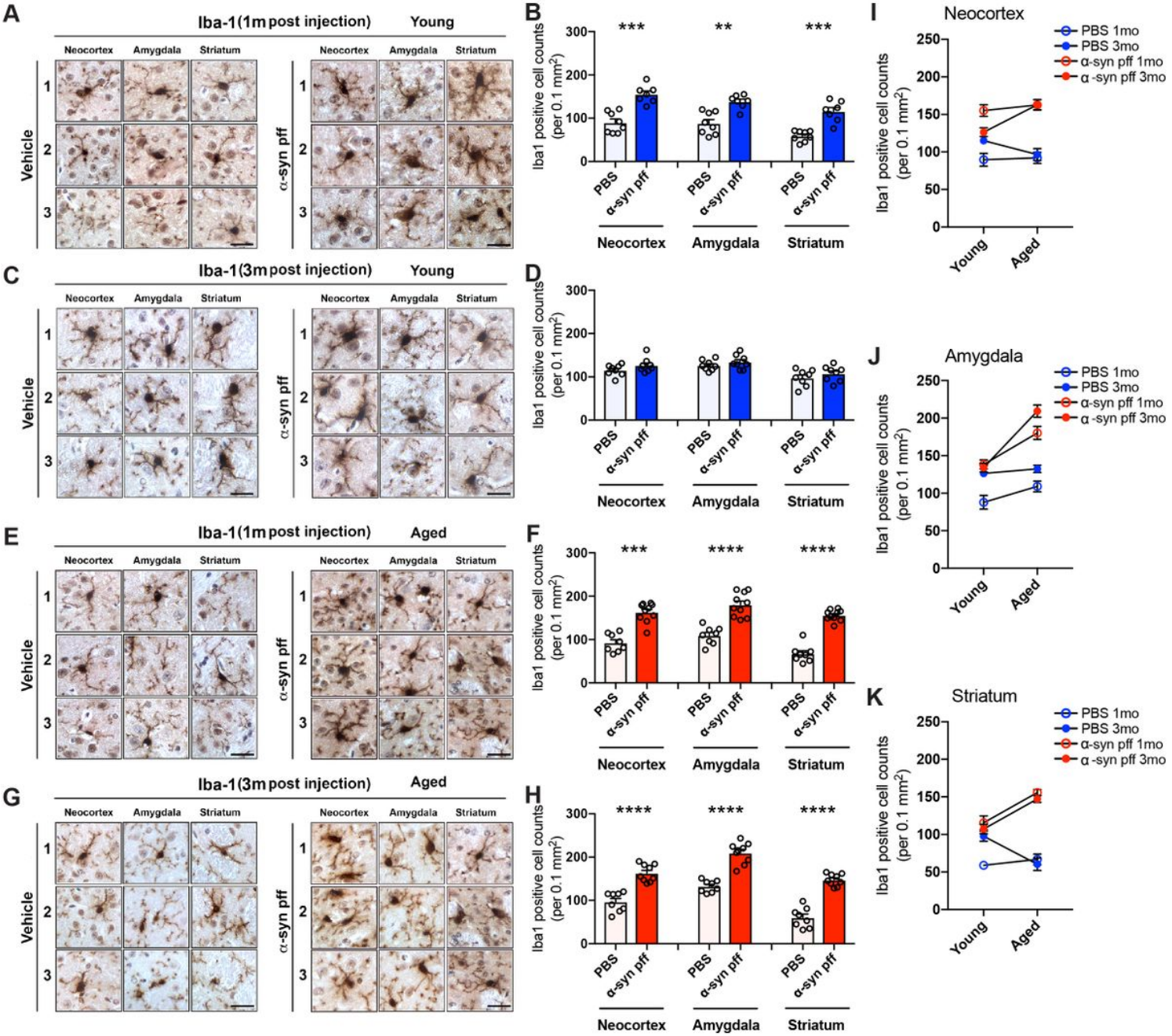

Figure 4

Immunohistochemical analysis of microglial cells with the Iba1 antibody in young and aged wt mice at 1- and 3-month post-injection with PBS or α-syn pff. (A) Representative images for Iba1 immunostaining in young mouse cohort at 1-month post injection. Images are from three different mice (1, 2 and 3) of three brain regions (cortex, amygdala, and striatum). Left panels are PBS (vehicle) injected and right are α-syn pff injected. (B) Image analysis of Iba1 positive cell counts per 0.1mm2 of young mouse cohort at 1-month post injection. (C) Iba1 immunostaining of young mouse cohort at 3-month post injection. Same format as A. (D) Image analysis of Iba1 positive cell counts per 0.1mm2 of young mouse cohort at 3-month post injection. (E) Iba1 immunostaining of aged mouse cohort at 1-month post injection. Same format as A. (F) Image analysis of Iba1 positive cell counts per 0.1mm2 of aged mouse cohort at 1-month post injection. (G) Iba1 immunostaining of aged mouse cohort at 3-month post injection. Same format as A. (H) Image analysis of Iba1 positive cell counts per 0.1mm2 of aged mouse cohort at 3-month post injection. (I-K) Comparison of image analysis of Iba1 positive cell counts per 0.1mm2 in cortex (I), amygdala (J) and amygdala (K) of α-syn pff injected mice at 1- and 3-month post-injection in young (blue) and aged (red) mouse cohorts. Scale bar is 20 mm. **p < 0.01; ***p < 0.001; ****p < 0.0001.

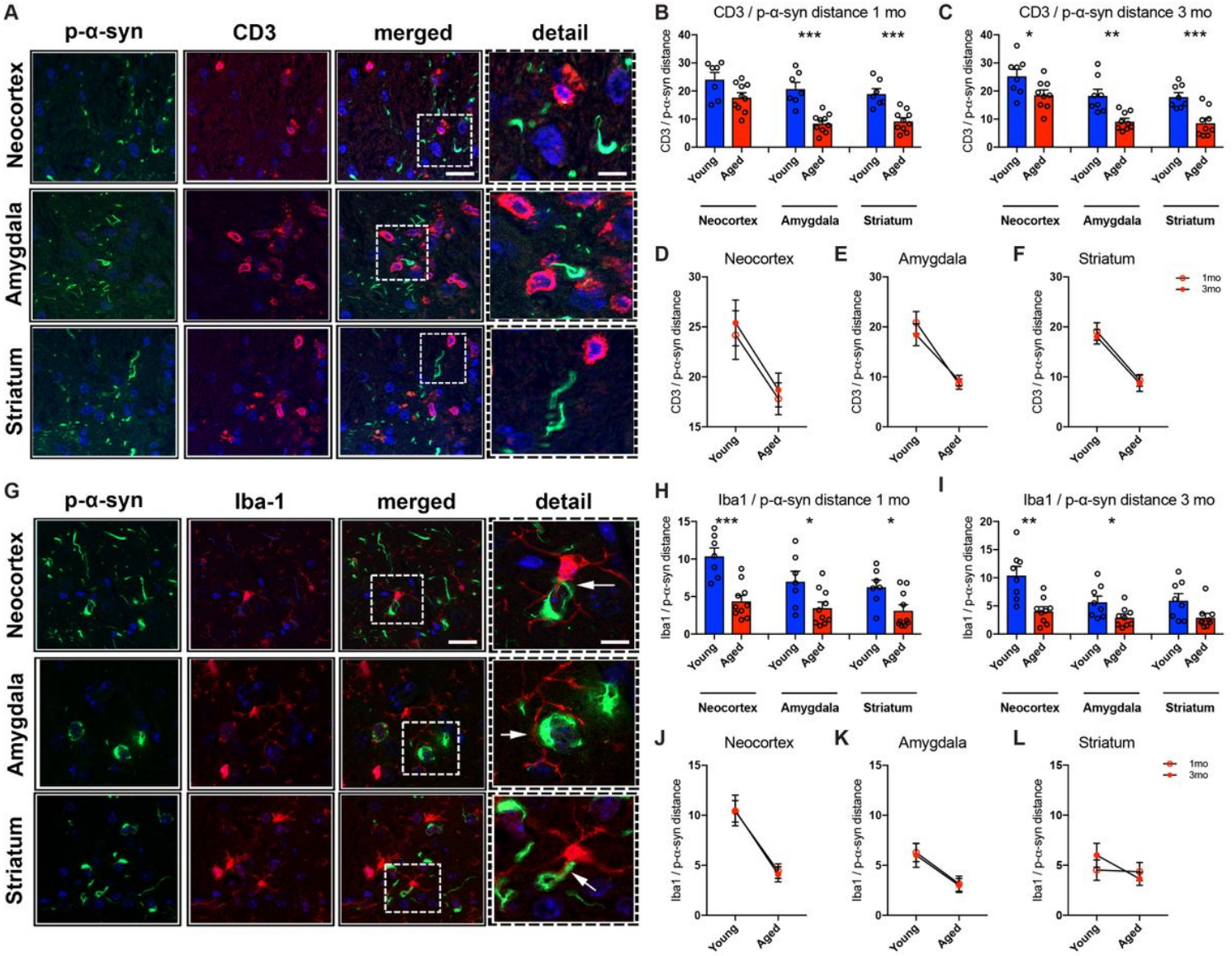

Figure 5

Double immune-fluorescence analysis for T cells or microglia and p-□-syn in young and aged wt mice at 1- and 3-month post-injection with □-syn pff. (A) Double immunofluorescence staining with phosphorylated □-syn (p-□-syn, 81A) and CD3 antibodies. Split and merged representative microscopy images from the neocortex, amygdala, and striatum of □-syn pff injected aged mouse double labeled with antibodies against p-□-syn (green) and CD3 cells (T cells, red channel). (B and C) Quantiative analysis of distances between p-□-syn and CD3 cells in neocortex, amygdala and striatum in 1-month (B) or 3-month (C) post injection. (D-F) Comparison of image analysis of proximity between p-□-syn and CD3 cells in neocortex, amygdala and striatum in young and aged mouce cohorts. (G) Double immunofluorescence staining with Iba1 and CD3 antibodies. Split and merged representative microscopy images from the neocortex, amygdala, and striatum of □-syn pff injected aged mouse double labeled with antibodies against p-□-syn (green) and Iba1 (microglia cells, red channel). (H and I) Quantiative analysis of distances between p-□-syn and microglia cells in neocortex, amygdala and striatum in 1-month (H) or 3-month (I) post injection. (J-L) Comparison of image analysis of proximity between p-□-syn and microglia cells in neocortex, amygdala and striatum in young and aged mouce cohorts. Scale bar is 20 mm in low magnification and 10 mm in the high magnification. * p < 0.05; ** p < 0.01; *** p < 0.001

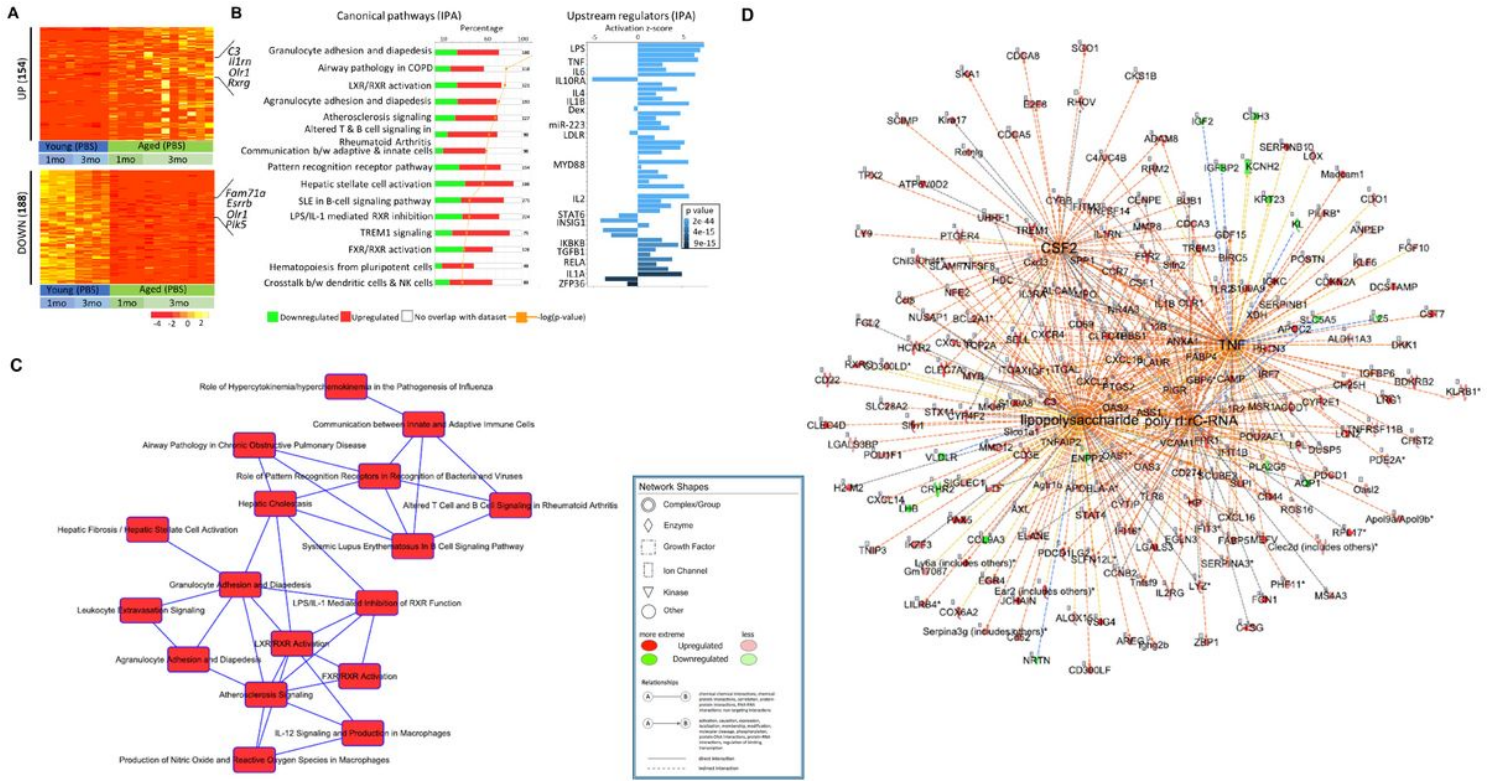

Figure 6

Characterization of age-associated genes in microglia. (A) RNA from microglia of PBS injected young and aged wt mice were compared to identify the age-associated differentially expressed genes (DEGs). The RNA-Seq identified 622 up- and 188 downregulated genes (> 2-fold change, p<0.05) (for visual purpose, 154 > 4-fold upregulated genes have been shown). For the age-associated comparison, PBS injected control mice from 1- and 3-months (including repeats) post injection groups were combined and the TpM normalized values of the DEGs are represented in the heatmap. The number of DEGs are mentioned on

the left of the heatmap with few of the prominent genes mentioned on the right. (B) The age-associated differentially expressed genes (both up- and downregulated genes) were analyzed with IPA to identify enriched canonical pathways (left), and upstream regulators of the genes (right). The canonical pathways show the most enriched biological processes along with the percentage of up-(red) and downregulated (green) genes in each pathway with total number of genes mentioned outside the bar graphs. The -log p-value from the enrichment analysis is represented by a yellow dot. The upstream regulator plot identifies the cascade of upstream transcriptional regulators whose expression is affected by aging. Prominent immune regulators are noted. The bar graph shows the activation Z-score where a positive score implies activation of the transcriptional regulator while the negative score indicates repression. The color of the bar graph represents the p-value. (C) Based on the canonical pathways derived from IPA, a network was constructed comprising of pathways with more than 5 common enriched genes (or other molecules) that changed with age. (D) Based on the transcriptional upstream regulators obtained from IPA, a network of the top upstream regulators (CSF2, LPS, TNF and poly rI:rC-RNA) and their target genes (or other molecules) was constructed. This plot shows how the upstream regulator networks overlap via their target genes.

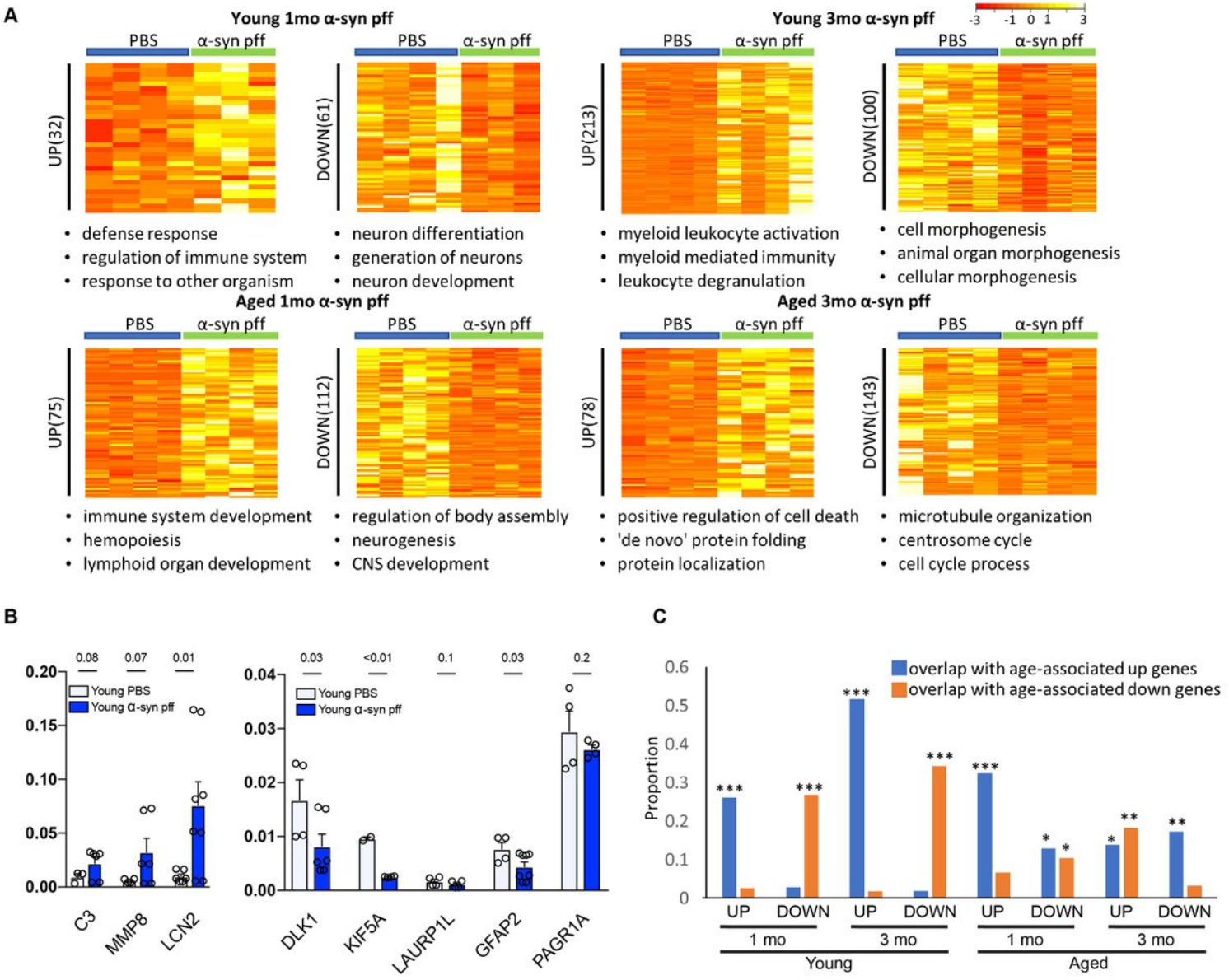

Figure 7

Effect of □-syn pff injection on microglial gene expression. (A) Genes dysregulated by 1- and 3-months of □-syn pff injection in young and aged mice were identified by DESeq2 (fold change > 2, p<0.05). The expression levels of the DEGs are represented as TpM normalized values for young mice in the upper row and for the aged mice in the lower row. The number of DEGs are indicated to the left of the heatmap. The top 3 pathways associated with each group were determined from ToppGene database as shown below the respective heatmaps. (B) RNA-Seq results were validated by qRT-PCR for selected candidates. Samples were analyzed in duplicate and expression levels were normalized against Gapdh. The mean and standard error are derived from combining all samples in a group. C3, Mmp8 and Lcn2 go up with □-syn pff injection while Dlk1, Kif5a, Laurp1l, Gfap2 and Pagr1a (need to change font in graphpad file. Gene names are in uppercase in the figures) go down with □-syn pff injection as also observed in RNA-Seq results. The p-value from the t-test between PBS and □-syn pff data is shown above the bar graphs. (C) Comparison of □-syn pff-induced genes with age-associated genes in microglia. Genes that were up- or downregulated in response to □-syn pff (X axis) were compared with genes up- (purple bars) or downregulated (orange bars) with age. Data shown is for young and aged mice as indicated 1or 3 months after □-syn pff injection. The significance of overlap (asterisk) was confirmed by hypergeometric test.

Supplementary Files

This is a list of supplementary files associated with this preprint. Click to download.

- SupplementalInformationIbaetal.docx